Dyes and Pigments 86 (2010) 182–189

Contents lists available at ScienceDirect

Dyes and Pigments

journal homepage: www.elsevier.com/locate/dyepig

Spectral, thermal and optical properties of metal(II)–azo complexes for optical recording media

Xiaoyi Li [a], Yiqun Wu [a,b,*], Donghong Gu [a], Fuxi Gan [a]

[a] Key Laboratory of High Power Laser Materials, Shanghai Institute of Optics and Fine Mechanics, Chinese Academy of Sciences, No. 390, Qinghe Road, Jiading District, Shanghai 201800, PR China
[b] Key Lab of Functional Inorganic Material Chemistry (Heilongjiang University), Ministry of Education, Haerbin 150080, PR China

ARTICLE INFO

Article history:
Received 28 November 2009
Received in revised form
6 January 2010
Accepted 7 January 2010
Available online 18 January 2010

Keywords:
Metal(II)–azo complex
Spin-coating film
Absorption spectra
Thermal property
Optical property
Blue-ray recording medium

ABSTRACT

A novel ligand, (Z)-1,5-dimethyl-4-(2-(3-methyl-5-oxo-1-phenyl-1H-pyrazol-4(5H)-ylidene)hydrazinyl)-2-phenyl-1,2-dihydropyrazol-3-one] and its metal(II)–azo complexes were synthesized and characterized using elemental analyses, proton NMR, electrospray ionization mass spectrometry, FT-IR and UV–visible absorption. Smooth thin films of the metal(II)–azo complexes were prepared using spin-coating, and the absorption spectra of the films were measured. The thermal properties of the metal (II)–azo complexes were investigated using TGA and DSC. The optical constants (complex refractive index $N = n + ik$) of the films on single-crystal silicon were determined using variable-angle scanning ellipsometry from which the complex dielectric function (ε) and absorption coefficient (α) were calculated. The photostabilities of the metal(II)–azo complex films were also investigated.

1. Introduction

Azo compounds are highly coloured that enjoy widespread use as dyes and pigments in a variety of applications that include textile dyeing [1] as well as non-linear and photoelectronics [2], especially in optical information storage [3–7]. Laser-based optical recording has developed significantly in recent years, recording being achieved in such a manner that upon absorption of the irradiating laser beam energy, a portion of the recording layer undergoes thermal deformation such as decomposition, evaporation or dissolution. Reproduction of the recorded information is secured by reading the difference in reflectance between the portion at which deformation was achieved and a portion where no deformation occurred. Accordingly, the optical recording medium is required to efficiently absorb the laser beam energy. Dyes have been used since 1985 as successors to inorganic Te materials for write-once optical memory discs; recordable compact discs (CD-R) optical recording elements based on an active dye layer such as that provided using selected cyanine dyes with added stabilizers as well as metal phthalocyanine dyes are widely known. Wang [8,9] reported metal(II)–azo complexes with suitable optical absorption at 780 nm and a high carrier-to-noise ratio of 45 dB which were suitable for use as optical CD-R recording media. Metal (II)–azo complexes have also been reported for use as optical recording media in digital versatile disc-recordable (DVD-R) media; various types have been patented and published [10–14]. In recent years, with the appearance of the 405 nm blue-ray semiconductor laser, optical recording media capable of recording information in high density by means of a laser beam of 405 nm rather than 635–650 nm are desired [15–17]. However, most dyes which are currently used in CD-R and DVD-R optical recording media are not applicable to 405 nm. Metal(II)–azo complexes used as high-density storage media, especially as blue-ray disc-recordable (BD-R) medium, have attracted a great deal of interest due to their blue-violet absorption, high solubility in organic solvents, good film-forming ability, high thermal stability and good optical character [7,18–20]. In order to achieve improved storage medium, various factors should be considered in the context of the synthesis of new recording materials, namely suitable optical absorption, sharp thermal decomposition threshold, high refractive index n and low extinction coefficient k of the dye film. Based upon the consideration of the above requirements, this paper concerns the synthesis of metal(II)–azo complexes (Fig. 1), NiL_2, CoL_2, CuL_2 and ZnL_2 [L = (Z)-1,5-dimethyl-4-(2-(3-methyl-5-oxo-1-phenyl-1H-pyrazol-4(5H)-ylidene)hydrazinyl)-2-phenyl-1,2-dihydropyrazo-3- one]. Results of the absorption and thermal properties, as well

* Corresponding author. Tel.: +86 21 69918087; fax: +86 21 69918562.
E-mail addresses: xyli@siom.ac.cn (X. Li), yqwu@siom.ac.cn (Y. Wu).

0143-7208/$ – see front matter
doi:10.1016/j.dyepig.2010.01.002

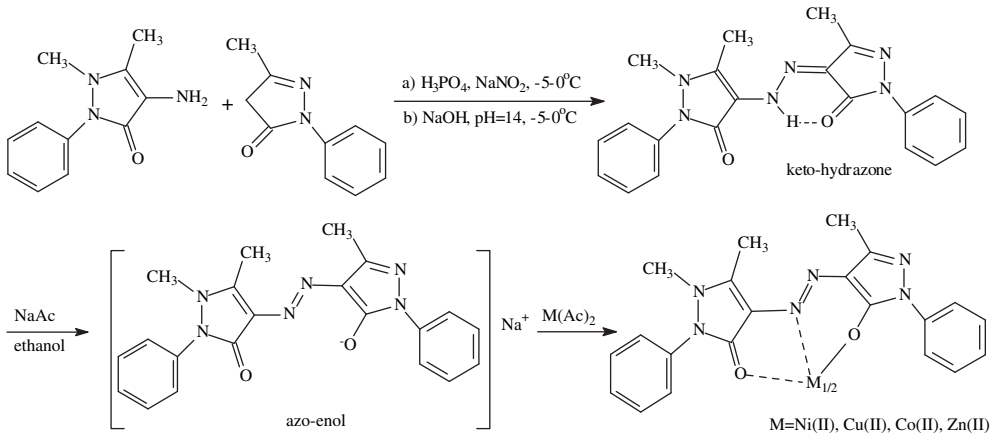

Fig. 1. Synthetic schemes of ligand and its metal(II)–azo complexes.

as optical characteristics of the metal(II)–azo complexes, indicate that the metal(II)–azo complexes are promising candidates for use as blue-ray optical recording media.

2. Experimental

2.1. Materials

All the reagents and solvents in this work were of reagent-grade quality. 4-aminoantipyrine and 3-methyl-1-phenyl-2-pyrazolin-5-one were purchased from Sinopyarm Chemical Reagent Co., Ltd. and used without further purification. A facile route was adopted in the synthesis of the ligand and its metal(II)–azo complexes and the synthetic schemes together with suggested structures are shown in Fig. 1.

2.2. Synthesis of the ligand (HL) and its metal(II)–azo complexes

2.2.1. Diazotization

4-aminoantipyrine (3.2518 g, 0.0160 mol) was dissolved in 40 mL concentrated phosphoric acid (85%) at room temperature. The solution was then cooled to −5 to 0 °C in an ice-salt bath and maintained at this temperature, solution of sodium nitrite (1.1109 g, 0.0161 mol) in water (10 ml) was added dropwise within 1h under continuous stirring and the mixture was stirred at 0–5 °C 1 h. The resulting diazonium solution was used directly in the coupling step.

2.2.2. Coupling

The coupling component (3-methyl-1-phenyl-2-pyrazolin-5-one, 2.8220 g, 0.0162 mol) was dissolved in 200 ml sodium hydroxide solution (2%, pH = 14) and cooled to −5 to 0 °C in an ice-salt bath. The above diazonium solution was added to the stirred coupling component solution at −5 to 0 °C over 30 min, maintaining the pH at 8–10. The mixture was allowed to rise to room temperature over 4 h and the pH was lowered to about 5. The precipitated solid was filtered with suction, washed with water and then vacuum dried. The rough product was finally purified by column chromatography and further recrystallized to give (Z)-1,5-dimethyl-4-(2-(3-methyl-5-oxo-1-phenyl-1H-pyrazol-4(5H)-ylidene)hydrazinyl)-2-phenyl-1,2-dihydropyrazol-3-one (HL). Yield: 5.034g (81%). mp. 186–190 °C. Anal. Calad (found) for $C_{21}H_{20}N_6O_2$: C, 64.94 (64.76); H, 5.19 (5.11); N, 21.64 (21.44). ^{1}H NMR (DMSO-d_6, TMS, δ ppm): 2.543 (s, 3H, C=C–CH_3), 2.312 (s, 3H, N=C–CH_3), 3.117 (s, 3H, N–CH_3), 7.160–7.973 (m, 10H, two phenyls), 13.157 (s, 1H, hydrazone NH). Electronic absorption spectrum (UV–vis) in chloroform: λ_{max} (logε) = 418 (4.44). FT-IR spectra ν (cm^{-1}): 3400, 3064, 2925, 1670, 1636, 1594, 1552, 1491, 1457, 1372, 1341, 1185, 1160, 1109, 1070, 909, 727, 572, 505. ESI-MS Calcd (found): m/z = 388.42 (389.3) [M + H^+].

2.2.3. Metallization

The resulting ligand (0.64 mmol) was dissolved in 40ml of ethanol together with 0.641 mmol of sodium acetate. After heating up to reflux, the metal(II) acetate (0.33 mmol) dissolved in 2 mL water was added dropwise under vigorous stirring, whereupon a suspension of the metal(II) complex dye results. The precipitated solid was collected by filtration, washed with water and then vacuum dried to obtain the metal(II)–azo complex. Specific details for each compound are given below.

2.2.3.1. NiL_2 complex. Yield: 81%. mp.> 297 °C. Anal. Calad (found) for $C_{42}H_{38}N_{12}O_4Ni$: C, 60.52 (60.40); H, 4.60 (4.55); N, 20.17 (20.21). Electronic absorption spectrum (UV–vis) in chloroform: λ_{max} (log ε) = 441 (4.58). FT-IR spectra ν (cm^{-1}): 3064, 2922, 1616, 1588, 1530, 1481, 1433, 1412, 1368, 1346, 1224, 1166, 1112, 1073, 902, 737, 580, 509, 480, 445. ESI-MS Calcd (found): m/z = 832.2 (833.1) [M + H^+].

2.2.3.2. CoL_2 complex. Yield: 92%. mp.> 279 °C. Anal. Calad (found) for $C_{42}H_{38}N_{12}O_4Co$: C, 60.50 (59.78); H, 4.59 (4.72); N, 20.16 (19.73). Electronic absorption spectrum (UV–vis) in chloroform: λ_{max} (logε) = 425 (4.60). FT-IR spectra ν (cm^{-1}): 3064, 2919, 1605, 1570, 1511, 1471, 1433, 1413, 1369, 1342, 1223, 1164, 1112, 1074, 904, 734, 578, 509, 465, 447. ESI-MS Calcd (found): m/z = 833.2 (834.1) [M + H^+].

2.2.3.3. CuL_2 complex. Yield: 84%. mp. > 281 °C. Anal. Calad (found) for $C_{42}H_{38}N_{12}O_4Cu$: C, 60.17 (60.07); H, 4.57 (4.50); N, 20.05 (19.83). Electronic absorption spectrum (UV–vis) in chloroform: λ_{max} (logε) = 437 (4.70). FT-IR spectra ν (cm^{-1}): 3062, 2921, 1616, 1589, 1535, 1473, 1440, 1417, 1368, 1338, 1302, 1265, 1190, 1170, 1144, 1109, 1072, 900, 735, 580, 509, 475, 440. ESI-MS Calcd (found): m/z = 837.2 (838.3) [M + H^+].

2.2.3.4. ZnL_2 complex. Yield: 84%. mp. > 279 °C. Anal. Calad (found) for $C_{42}H_{38}N_{12}O_4Zn$: C, 60.04 (59.59); H, 4.56 (4.54); N, 20.00 (19.76). Electronic absorption spectrum (UV–vis) in chloroform: λ_{max} (logε) = 441 (4.74). FT-IR spectra ν (cm^{-1}): 3065, 2921, 1612, 1590, 1566, 1476, 1435, 1415, 1368, 1340, 1289, 1222, 1164, 1111, 1073, 902, 734, 580, 508, 463, 441. ESI-MS Calcd (found): m/z = 838.2 (839.0) [M + H^+].

2.3. Preparation of the spin-coated thin films

The solutions were prepared by dissolving the respective metal (II)–azo complex in 2,2,3,3-tetrafluoro-L-propanol (TFP) to give a concentration of 30 mg mL^{-1} solution. The solution was filtered using a 0.22 μm Millipore membrane filter to obtain the coating solution. The K9 glass and single-crystal silicon wafers (diameter 30 mm) were used as substrates and were cleaned by being immersed in piranha solution (3:1 concentrated H_2SO_4/30% H_2O_2) for 3 h at 80 °C. They were then rinsed repeatedly with deionized water and ethanol in an ultrasonic bath and dried, successively. Smooth thin films were easily prepared by spin-coating at a two-step procedure, 400 rpm for the first 3 s and 2600 rpm thereafter for 40 s, with a KW-4A precision spin-coater (Chemat Technology Inc.) using a syringe. The substrates were kept at room temperature and 50% relative humidity throughout the deposition process. The resulting films were then heated at 50 °C for 2–3 h to ensure removal of the solvent.

2.4. Instrument and methods

The melting points of the compounds were determined using an XT-4 microscopic melting point apparatus (made in China) and were uncorrected. Elemental analyses of C, H and N were carried out on a Vario EL elemental analyzer. The Fourier Transform Infrared (FT-IR) spectra were obtained in KBr pellets on a Perkin–Elmer FT-IR 1650 spectrometer in the 4000–400 cm^{-1} region. ^1H NMR spectra ($CDCl_3$ solutions) were recorded on a Brucker AV 500 MHz Spectrometer in $CDCl_3$ using TMS as an internal reference. The electrospray ionization (ESI) mass spectra were performed using a Surveyor LCQ spectrometer. The Ultraviolet–visible (UV–vis) spectra were measured using a Perkin–Elmer Lambda 9UV/VIS/NIR spectrophotometer. Thermal properties were analyzed with a TA instrument, the SDT Q600 Simultaneous DSC/TGA Analyzer, at a heating rate of 10 °C min^{-1} from 50 to 700 °C under nitrogen atmosphere. The measurements of optical constants (*n* and k) and the thicknesses of thin films were performed by variable-angle scanning ellipsometry (Rotating Analyzer-Polarizer-1, Fudan University and D&G Instrument) in air at atmospheric pressure and at room temperature for incident angles in 65°–75° with 5° interval and for wavelength from 275 nm to 695 nm with 10 nm interval. The dependence of the optical constants (*n* and k) of the thin films on the wavelength in the range 275–695 nm and the thicknesses of thin films were done using the Film Wizard™ software available from the Scientific Computing International by minimizing the difference between the experimental data ψ^{exp} and Δ^{exp}, and the model data ψ^{mod} and Δ^{mod}. The two parameters, ψ and Δ, appeared as functions of the wavelength (or photon energy) and angle of incidence in the scanning ellipsometry measurements. A detailed description of the operation principles and experimental procedures can be found in Refs. [21,22]. The potostabilities of the metal–azo complexes films was carried out using a setup for blue-ray optical recording with 406.7 nm krypton and mixed-gas ion laser and 0.90 numerical aperture objective lens under the reading laser radiation.

3. Results and discussion

3.1. Synthesis and characterization

The ligand was synthesized by diazo coupling reaction. It may exist in keto-hydrazone and azo-enol tautomeric forms as shown in Fig. 1. It has bee shown, conclusively from a series of investigations using various techniques, such as IR, NMR and X-ray crystallography, that hydrazones containing 5-pyrazolone groups exist exclusively in the keto-hydrazone form both in solution and in the solid state [23–25]. An intramolecular hydrogen bridge linking one of the carbonyl groups to the NH-moiety of the hydrazone unit was found to be a characteristic feature of this compound class. The six-membered intramolecular hydrogen bonding ring is possible in the keto-hydrazone tautomer as showed in Fig. 1. The infrared spectra of hydrazone based on a substituted 5-pyrazolone and, in particular the position of the carbonyl stretching vibrations, have been of considerable importance in establishing that the compounds exist exclusively in the keto-hydrazone form. The solid state IR spectra of the synthesized ligand shows two intense carbonyl bands (1670 (νC=O···H), 1636 (νC=O) cm^{-1}) consistent with a keto-hydrazone form. It can be suggested that the ligand exists as keto-hydrazone form with extensive six-membered intramolecular hydrogen bonding, and this has been confirmed by a number of previous published reports of keto-hydrazone analogues [26–28]. Another typical feature of the free ligand is the existence of an NH vibration around 3400 cm^{-1} which affords proof of the H-bonded hydrazone structure in the solid state also [23,29]; the remaining vibrational frequencies obtained and their tentative assignments are shown in Table 1. In the ^1H NMR spectra of the ligand measured in $CDCl_3$, the hydrazone proton appears as a singlet at 13.157 ppm, which corresponds to imine NH proton resonance of the hydrazone form [30]. The above results suggest that the ligand prepared exists in the keto-hydrazone form in the solid state, and the obtained IR spectra, ESI mass spectra, ^1H NMR and elemental analytical data agree well with the formulae of the ligand.

The metal(II)–azo complexes were synthesized by reaction of the relevant metal(II) acetate with the ligand. Due to the possible keto-hydrazone and azo-enol tautomerism of the prepared ligand [23], the action of the sodium acetate on the ligand in solution is to convert the keto-hydrazone form into the azoanion form [25,31]. Consequently, metal(II)–azo complexes were easily synthesized by the chelation of the metal(II) ion and ligand in the azo-enol form (see Fig. 1). The elemental analytical data, ESI mass spectra and FT-IR spectra of the metal(II)–azo complexes agree well with their formulae. The metal-to-ligand ratios of the metal(II)–azo complexes were found to be 1:2. Fig. 1 shows the suggested structure of the metal(II)–azo complexes.

3.2. FT-IR spectra of the ligand and its metal(II)–azo complexes

The important IR characteristic absorption bands, along with their proposed assignments, are summarized in Table 1. As seen from Table 1, the IR spectra of the metal(II)–azo complexes were similar to each other, except for some slight shifts and intensity

Table 1
Significant FT-IR bands and tentative assignments of the ligand and its metal(II)–azo complexes.

Compound	νH–N (hydrazone)	νAro–H	νAl–H	νC=O	νN=N	νC–O(enol hydroxyl)	νM–N	νM–O
HL	3400	3064	2925	1670, 1636	–	–	–	–
$Ni(L)_2$	–	3061	2922	1616	1412	1224	445	480
$Co(L)_2$	–	3064	2919	1605	1413	1223	447	465
$Cu(L)_2$	–	3062	2921	1612	1417	1265	440	475
$Zn(L)_2$	–	3065	2921	1612	1415	1222	431	463

changes of a few vibration bands caused by different metal(II) ions, which indicates that the complexes were of similar structure. However, there were some significant differences between the free ligand and the metal(II)–azo complexes. The coordination mode and sites of the ligand to the metal(II) ions were investigated by comparing the infrared spectra of the free ligand with its metal (II)–azo complexes. Upon coordination, it is noteworthy that one strong absorption bands in the region 1605–1616 cm^{-1} attributed to νC=O vibration were shifted by 20–31 cm^{-1} on complexation, while the second carbonyl absorption band at 1670 cm^{-1}, appearing in the spectra of the free ligand with the extensive six-membered intramolecular hydrogen bonded structure, was not observed. These results indicate that the ligand is in the azo-enol form in the complex which naturally forms an enolic hydroxyl oxygen and an enolic carbony with consequent replacement of the enolic hydrogen by the metal(II) ion [32]. A new band due to C–O vibration appearing at 1222–1265 cm^{-1} in the spectra of all the metal(II)–azo complexes can be further evidence for the bonding of the enol hydroxyl oxygen to the metal(II) ion [30,33]. Furthermore, the medium-intensity band at 3400 cm^{-1} of the free ligand, due to νNH stretching, disappears in the complexes, suggesting that the NH proton is lost via enolization and the resulting enolic oxygen and azoic nitrogen take part in coordination [34]. Moreover, another new band due to –N=N– vibration appears around 1412–1417 cm^{-1} in the spectra of all the complexes, which supports the azo-enol form of the ligand in the metal(II) complexes; the appearance of this peak at relatively lower field may indicate coordination via the N=N group [32,35,36]. In addition, the IR spectrum of the ligand reveals a sharp band at about 1636 cm^{-1} corresponding to the νC=O of the antipyrine ring, which was shifted to a lower frequency by about 20–31 cm^{-1} after complexation in all metal(II)–azo complexes, suggesting that the oxygen atom of the antipyrine ring also contributes to complexation [30,37]. The mode of bonding of the metal(II) ion is further supported by the broad absorption bands in the region 463–480 and 431–447 cm^{-1}, which can be assigned to νM–O and νM–N stretching vibrations, respectively [36,38]. Therefore, from these IR spectra, it is concluded that the ligand may exist in azo-enol form during complexation and behave as an O,N,O′–monobasic tridentate ligand coordinated to metal(II) ions via the enolic hydroxyl O, azoic group N and O of the antipyrine ring.

3.3. UV–vis electronic absorption spectra of the ligand and its metal(II)–azo complexes

The formation of the metal(II)–azo complexes was also confirmed by UV–vis spectra. Fig. 2 gives the absorption spectra of the ligand and its metal(II)–azo complexes in chloroform solutions. It is known that the ligand has two absorption bands. The first band appearing below 250 nm is attributed to $\pi \rightarrow \pi^*$ transition of the heterocyclic moiety and phenyl ring [39,40]. The second band appearing around 418 nm arises from a transition involving electron migration along the entire conjugate system of the ligand [40]. In the spectra of the metal(II)–azo complexes, the absorption bands are shifted to higher wavelengths relative to their metal free ligand. From Fig. 2, it also can be observed that the maximal absorption peak of the free ligand is at 418 nm, but those of its metal(II)–azo complexes are at 425, 437, 440 and 441nm for CoL_2, NiL_2, CuL_2 and ZnL_2, and bathochromic shift 7, 19, 22 and 23 nm comparative to the free ligand, respectively. This also indicates that center metal ions have influence on the absorption bands of the complexes. According to modern molecular orbital theory [41], any factor, such as the electronegativity, the radius and electronic configuration of the metal(II) ion, that can influence the electronic density of a conjugated system must result in the difference of the

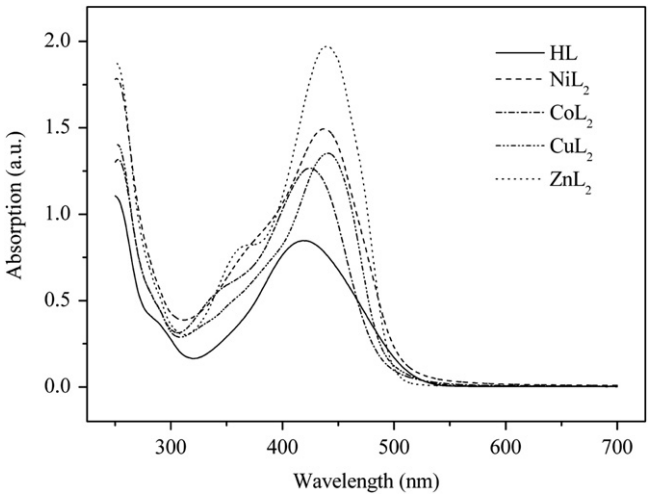

Fig. 2. Absorption spectra of the ligand and its metal(II)–azo complexes in chloroform.

absorption band. For metal(II) ions, in general, the ability to attract the electron enhances with the electronegativity increasing and the radii reducing. In the complexes CoL_2, NiL_2, CuL_2, the order of electronegativity metal(II) ions is 1.88 $Co^{2+}(d^7)$ < 1.91 $Ni^{2+}(d^8)$ < 2.0 $Cu^{2+}(d^9)$, the order of radii is Co^{2+} (0.74 Å)> Ni^{2+} (0.72 Å)> Cu^{2+} (0.69 Å), so the ability to attract the electrons from the oxygen and nitrogen should be Co(II) < Ni (II) < Cu (II), the energy gaps of $\pi \rightarrow \pi^*$ is reduced from CoL_2 to CuL_2. Therefore, the bathochromic shift is $CuL_2 > NiL_2 > CoL_2$, which is well in agreement with our experiment results. For ZnL_2 complex, because of its fully filled d-orbit (d^{10}), its electronegativity (1.6) and radius (0.74 Å) probably work in combination with and contribute to the absorption band shift.

We also prepared solid thin films of the metal(II)–azo complexes on K9 substrates by spin-coating and investigated the absorption spectra of the thin films. As shown in Fig. 3, the thin films show similar absorption bands compared with those obtained in chloroform solution. However, the slightly shifts of the absorption bands are also observed. These changes originate from extensive excitation coupling between adjacent conjugated molecules, as observed earlier in other complexes [7]. The metal(II)–azo complex films show suitable electronic absorption spectra with blue-violet light absorption at about 430–444 nm, which have an absorption on the 405 nm side. Therefore, these characteristics indicate that the metal(II)–azo complexes can have potential application for blue-ray optical recording media.

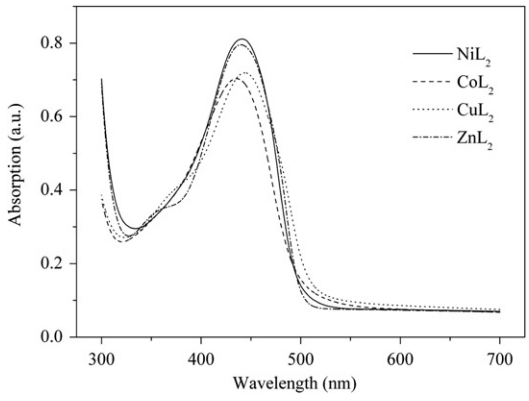

Fig. 3. Absorption spectra of the metal(II)–azo complex films on K9 glass substrates.

3.4. Thermal properties of the metal(II)–azo complexes

The thermal properties of the metal(II)–azo complexes were investigated by thermogravimetric (TG) analysis, differential thermogravimetric (DTG) and differential scanning calorimetry (DSC) in the temperature range 50–700 °C. Fig. 4 presents the recorded TG/DTG and DSC curves of the metal(II)–azo complexes in nitrogen atmosphere. The thermal analyses data for the metal(II)–azo complexes are summarized in Table 2. From the Fig. 4 and Table 2, it can be seen that the TG curves of the complexes show no any mass loss up to 230 °C, indicating the absence of water molecule and any other adsorptive solvent molecules in the coordination sphere. As the temperature is increased, the TG/DTG curves of the metal(II)–azo complexes exhibit a sharp mass loss at temperature of about 230–310 °C, which are accompanied with a sharp exothermic peak in the DSC curves. The correlations between the different decomposition steps of the metal(II) complexes with the corresponding mass losses are discussed in terms of the proposed formulae of the metal(II)–azo complexes.

From the TG curve of the NiL_2 complex, it can be seen that decomposition starts at 295.0 °C and shows almost a continuous weight loss in the temperature range of 295.0–700 °C. Based on the percentage of mass losses and the DTG curve, two-step decomposition is proposed for this complex, which is similar to the decomposition pattern reported previously in the literature [7]. According to literature the azo bonds in the azo metal complexes breakdown when the temperature is higher than 250 °C resulting in the exothermic peaks [25]. The first decomposition step with an estimated mass loss of 26.84% within the temperature range 295.0–313.2 °C may be attributed to the loss of $C_{11}H_{11}N_3O$ molecule (calcd. 24.14%). The DTG peak corresponding to this stage is at 301.9 °C and the recorded DSC curve reveals a sharp exothermic peak at 303.0 °C. The second step of decomposition occurs after the rapid mass loss with an estimated mass loss of 38.12%, which may correspond to the degradation of the residual ligand molecules. But this decomposition process shows no obvious peaks both in the DTG and DSC curves.

The CoL_2 complex is thermally decomposed in four successive decomposition steps within the temperature range 50–700 °C. The first decomposition step of estimated mass loss 22.14% within the temperature range 230.0–315.8 °C may be attributed to the loss of the $C_{11}H_{11}N_3O$ molecule (calcd. 24.14%). Three DTG peaks corresponding to this stage are observed at 267.3, 273.0 and 280.1 °C, respectively. Simultaneously, the recorded DSC curve reveals a broad exothermic peak at 277.2 °C. The second step at the temperature range 315.8–388.8 °C with the mass loss 14.49% corresponds to the loss of the $C_5H_6N_3O$ molecule (calcd. 14.90%). This decomposition process shows a broad peak at 337.8 °C in the DTG curve. The third step found within the temperature range 388.8–484.9 °C with an estimated mass loss 17.32% which may be attributed to the loss of two phenyl molecules (calcd. 18.47%). The broad DTG peak corresponding to this step is observed at 449.4 °C. The recorded DSC curve shows no obvious peak. The remaining decomposition step with an estimated mass loss 18.06% is roughly assigned to the loss of residual ligand molecules. The broad DTG peak corresponding to this stage is observed at 583.6 °C. However, DSC curve shows no obvious peak.

The CuL_2 complex is thermally decomposed in two decomposition steps. The first decomposition step of estimated mass loss 15.23% within the temperature range 267.3–283.2 °C may be attributed to the loss of the $C_5H_6N_3O$ molecule (calcd. 14.82%). The DTG peak corresponding to this stage is observed at 274.8 °C. The recorded DSC curve reveals sharp exothermic peak at 275.0 °C. The second step occurs within the temperature range 283.2–700 °C with an estimated mass loss 44.34, which may be due to the

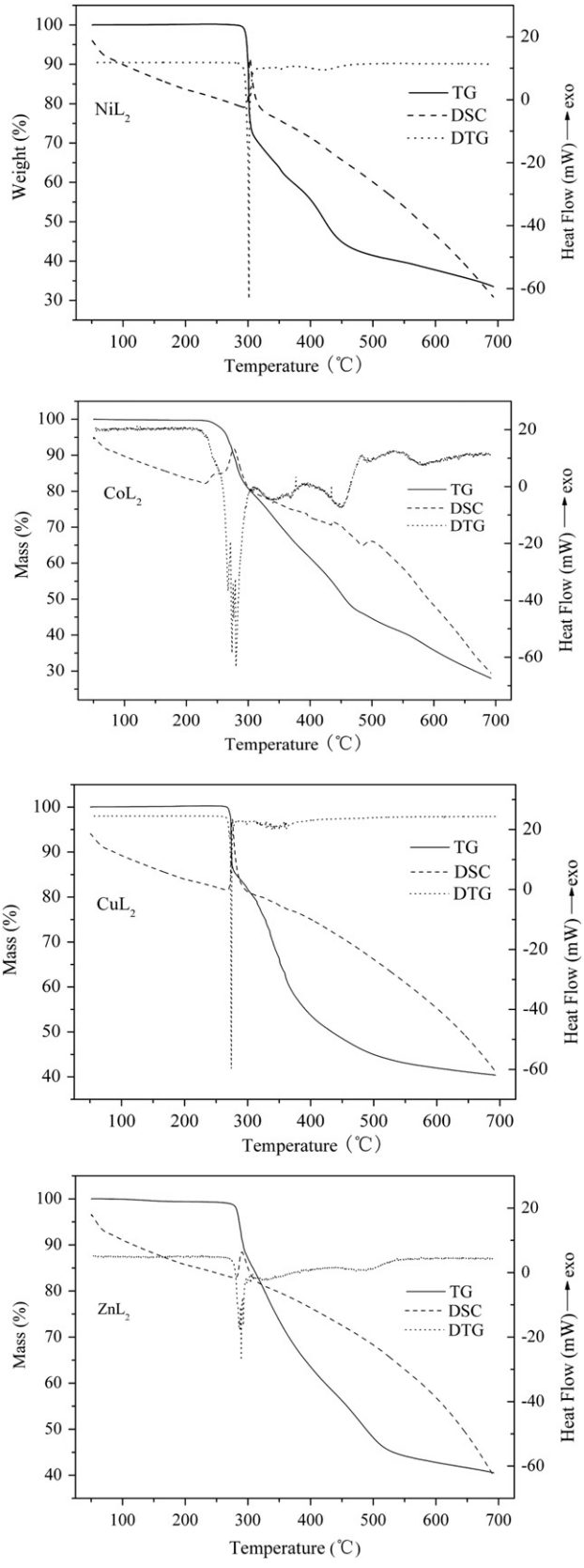

Fig. 4. TG/DTG and DSC curves of the metal(II)–azo complexes.

Table 2
Thermal analyses data for the metal(II)–azo complexes.

Compound	Dissociation stages	Temperature Range (°C)	Mass loss Found (calcd.) (%)	DTG peak (°C)	DSC peak (°C)	Decomposition assignment
NiL_2	Stage I	295.0–313.0	26.84 (24.14)	301.9	303.0	The loss of $C_{11}H_{11}N_3O$
	Stage II	313.0–700	38.12 (–)	–	–	The loss of residual ligand
CoL_2	Stage I	230.0–315.8	22.14 (24.14)	267.3, 273.0, 280.1	277.2	The loss of $C_{11}H_{11}N_3O$
	Stage II	315.8–388.8	14.49 (14.90)	337.8	–	The loss of $C_5H_6N_3O$
	Stage III	388.8–484.9	17.32 (18.47)	449.4	–	The loss of two phenyl molecules
	Stage IV	484.9–700	18.06 (–)	583.6	–	The loss of residual ligand
CuL_2	Stage I	267.3–283.2	15.23 (14.82)	274.8	275.0	The loss of $C_5H_6N_3O$
	Stage II	283.2–700	44.34 (46.33)	–	–	The loss of one ligand
ZnL_2	Stage I	278.4–305.3	14.30 (14.79)	289.9	291.4	The loss of $C_5H_6N_3O$
	Stage II	305.3–700	45.16 (46.23)	–	–	The loss of one ligand

decomposition of one ligand molecule (46.33%), and shows no obvious peaks in the DTG and DSC curves.

The ZnL_2 complex also shows decomposition pattern of two stages. The first step displays a mass loss of 14.30% within the temperature range 278.4–305.3 °C with a DTG peak at 289.9 °C, which may be attributed to the loss of the $C_5H_6N_3O$ molecule (calcd. 14.79%). The recorded DSC curve reveals an exothermic peak at 291.4 °C. The second step exhibits a gradual loss in mass within the remaining temperature range with the mass loss of 45.09%, which may be attributed to the decomposition of one ligand molecule (46.23%). This step shows no obvious peaks in the DTG and DSC curves.

The above TG and DTG data reveal that the decomposition pattern is different. The NiL_2, CuL_2 and ZnL_2 complexes exhibit only two-step decomposition, whereas four-stage decomposition is observed in the case of CoL_2 complex. According to the onset temperatures extrapolated from TG curves the following order of thermal stability may be proposed: $NiL_2 > ZnL_2 > CuL_2 > CoL_2$. The difference in thermal stability of the metal(II)–azo complexes may be due to the stereostructure of the metal(II)–azo complexes and electronic configuration of the metal(II) ion. In addition, from the Fig. 4 and Table 2, it is clear that the synthesized complexes, especially NiL_2 and CuL_2 complexes have high thermal stability and a sharp thermal decomposition threshold, which offer the potential to form a small and sharp recording mark edge [7]. With further development, these complexes may ultimately prove to be an important class of blue-violet light recordable optical disk storage materials.

3.5. The optical properties of the metal(II)–azo complex films

The optical properties of the metal(II)–azo complexes thin films can be described by the complex refractive indices N and complex dielectric function ε ($\varepsilon = \varepsilon_1 + i\varepsilon_2$). The ellipsometric spectra of the metal(II)–azo complexe thin films, spin-coated on single-crystal silicon, were investigated on a scanning ellipsometer. The thicknesses of the metal(II)–azo complex thin films were simulated synchronously from the measured ellipsometric parameters using the Film Wizard Software to be 114, 104, 109 and 115 nm for NiL_2, CoL_2, CuL_2 and ZnL_2, respectively. The variation of refractive index N ($N = n + ik$) with wavelengths (λ) was obtained. Fig. 5 gives the real part n and imaginary part k of the complex refractive index of the films in the visible and near-IR regions. As shown in Fig. 5, the thin films of the metal(II)–azo complexes give the n values of 1.43–1.53

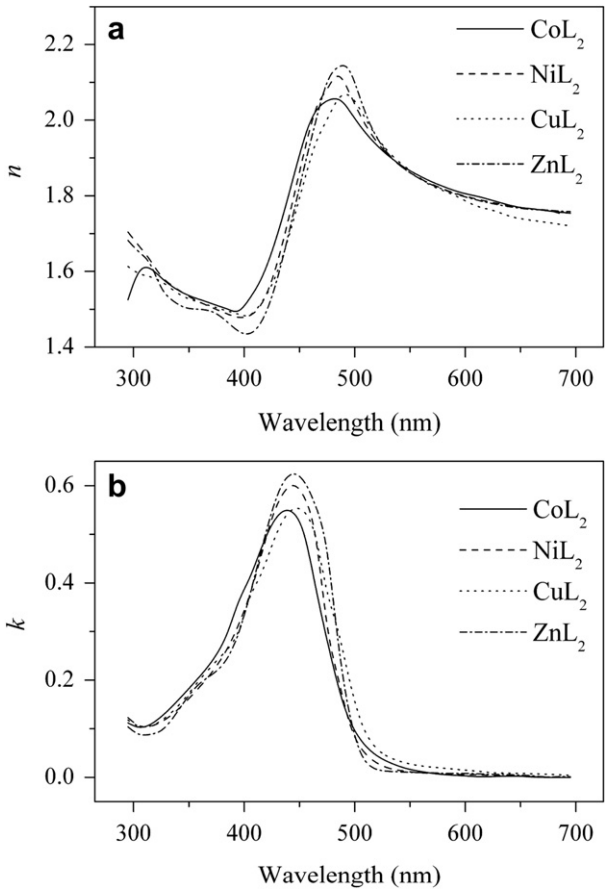

Fig. 5. Variation in refractive indices n and extinctive coefficients k as a function of wavelength for the thin films of the metal(II)–azo complexes.

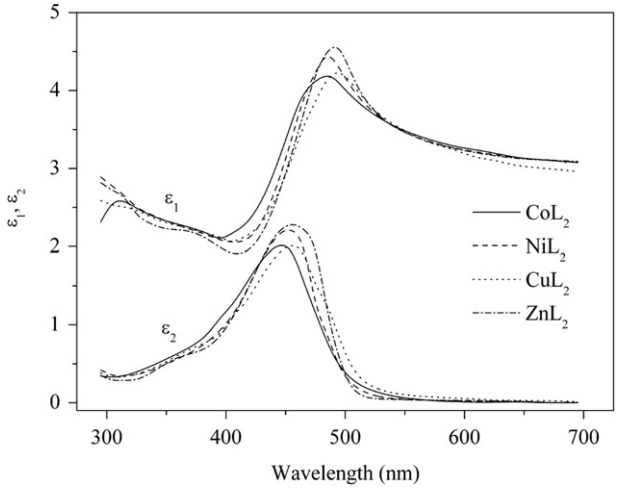

Fig. 6. Variation in real parts ε_1 and imaginary parts ε_2 of dielectric function as a function of wavelength for the thin films of the metal(II)–azo complexes.

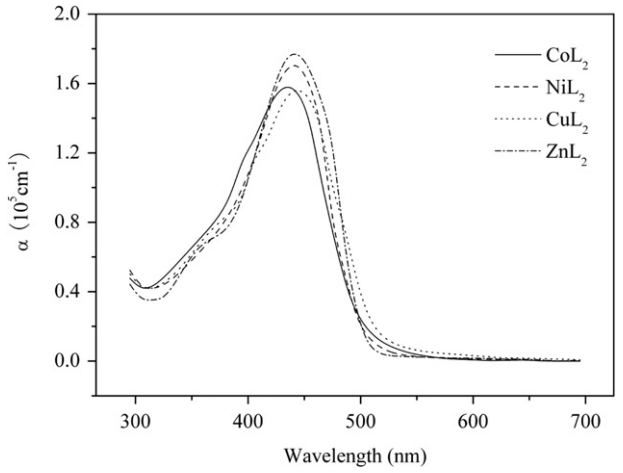

Fig. 7. Absorption coefficients α as a function of wavelength for the thin films of the metal(II)–azo complexes.

and k values of 0.37–0.41, respectively, corresponding to the output wavelength of the GaN laser diodes of 405 nm. In general, the real part n is related to the dispersion, while the imaginary part k provides a measurement of dissipation rate of the electromagnetic wave in the dielectric medium [42], and a high n value and a low k value can be helpful to obtain high optical recording signal modulation and high reflectivity R at writing wavelength of laser [5,43].

The real part ε_1 and imaginary part ε_2 of the complex dielectric function ε ($\varepsilon = \varepsilon_1 + i\varepsilon_2$) are related to the n and k of the complex refractive index by the following two equations respectively: $\varepsilon_1 = n^2 - k^2$, $\varepsilon_2 = 2nk$. From the values of n and k, the values of ε_1 and ε_2 can be calculated, and are shown in Fig. 6. The thin films of the metal(II)–azo complexes give real part ε_1 values of 1.90–2.17, and imaginary part ε_2 values of 1.07–1.24, respectively, at 405 nm. The absorption coefficient α can also be calculated from the expression $\alpha = 4\pi k/\lambda = 2\pi\varepsilon_2/\lambda n$. Fig. 7 shows the relationship of the absorption coefficient α (in the scale of 10^5 cm^{-1}) versus wavelength and gives α value of 1.15×10^5–1.26×10^5 cm^{-1} at 405 nm. It can be observed that the curves of the extinctive coefficient k and the imaginary part ε_2 of the complex dielectric function ε for the same thin film are structurally similar to the absorption spectra, and this has been confirmed by previous published results [44,45].

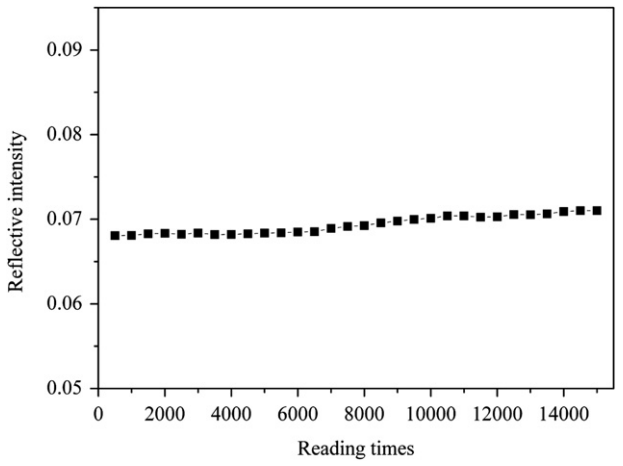

Fig. 8. The dependence of reflective intensity on reading times for the recording marks of CoL_2 complex film.

3.6. The photostabilities of the metal(II)–azo complex films

The metal(II)–azo complex films were prepared on a K9 glass substrate with Ag reflective layer by a spin-coating method. The photostabilities of metal(II)–azo complex films were carried out for static optical recording test using a 406.7 nm blue-violet laser and a high numerical aperture of 0.9 under writing power 2 mW, writing pulse width 300ns, reading power 0.5 mW. The reflective light intensities of metal(II)–azo complex films show no obvious change after 15 000 reading times on the recording marks, which indicates that the recording marks are photostable. Fig. 8 shows an example of reflective light intensity of the CoL_2 complex film as a function of reading times.

4. Conclusions

We have described the synthesis and some spectroscopic, thermal and optical properties. The possible structures of the ligand and its metal(II)–azo complexes were proposed based on elemental analyses, ^{1}H NMR, ESI-MS, FT-IR spectra and UV–vis electronic absorption. Suitable electronic absorption spectra of the metal(II)–azo complex films were found in blue-violet region of 350–450 nm. The thermal properties of the metal(II)–azo complexes show high thermal stability and the order of their thermal stability found is $NiL_2 > ZnL_2 > CuL_2 > CoL_2$. The optical properties of the metal(II)–azo complex films were characterized by the complex refractive indices N ($N = n + ik$) and complex dielectric constant ε ($\varepsilon = \varepsilon_1 + i\varepsilon_2$) in 275–695 nm. At 405 nm, the metal(II)–azo complex films give high n values of 1.43–1.53 and low k values of 0.37–0.41, dielectric constant real part ε_1 values of 1.90–2.17 and imaginary part ε_2 values of 1.07–1.24. In addition, the metal(II)–azo complex films have good photostability. The above results imply that these new metal(II)–azo complexes are promising organic recording media for the blue-ray optical storage system.

Acknowledgements

Financial support from the National Natural Science Foundation of China (No. 60490290), Chinese Academy of Sciences (KJCX2.YW. M06) and the National Science and Technology Program of China (No. 2007AA03Z412) is gratefully acknowledged.

References

[1] Koh J, Greaves AJ. Synthesis and application of an alkali-clearable azo disperse dye containing a fluorosulfonyl group and analysis of its alkali-hydrolysis kinetics. Dyes and Pigments 2001;50:117–26.
[2] Katz HE, Singer KD, Sohn JE, Dirk CW, King LA, Gordon HM. Greatly enhanced second-order nonlinear optical susceptibilities in donor-acceptor organic molecules. Journal of the American Chemical Society 1987;109(21):6561–3.
[3] Wang S, Shen S, Xu H. Synthesis, spectroscopic and thermal properties of a series of azo metal chelate dyes. Dyes and Pigments 2000;44:195–8.
[4] Li XY, Wu YQ, Gu DH, Gan FX. Optical characterization and blu-ray recording properties of metal(II) azo barbituric acid complex films. Materials Science Engineering B 2009;158:53–7.
[5] Gan FX, Hou LS, Wang GB, Liu HY. Optical and recording properties of short wavelength optical storage materials. Materials Science Engineering B 2000;76:63–8.
[6] Sabi Y, Tamada S, Iwamura T, Oyamada M, Bruder F, Oster R, et al. Development of organic recording media for blue high numerical aperture optical disc system. Japanese Journal of Applied Physics 2003;42:1056–8.
[7] Chen ZM, Wu YQ, Gu DH, Gan FX. Nickel(II) and copper(II) complexes containing 2-(2-(5-substitued isoxazol-3-yl)hydrazono)-5,5-dimethylcyclohexane-1,3-dione ligands: synthesis, spectral and thermal characterizations. Dyes and Pigments 2008;76:624–31.
[8] Wang SQ, Shen SY, Xu HJ, Gu DH, Yin JL, Tang XD. Synthesis and optical properties of an azo metal chelate compound for optical recording medium. Dyes and Pigments 1999;42:173–7.

[9] Wang SQ, Shen SY, Xu HJ, Gu DH, Yin JL, Tang XD. Spectroscopic and optical properties of an azo-metal chelate dye as optical recording medium. Materials Science and Engineering B 2000;76(1):69–72.
[10] Tsutomu S, Yasunobu U. Optical recording medium. JP2001180119, 2001.
[11] Yasuhiro A, Yasunobu U. Optical recording medium. JP2002144724, 2002.
[12] Geng YY, Gu DH, Gan FX. Spectral and optical recording properties of azo nickel thin film. Material Science and Engineering B 2004;110:115–8.
[13] Park H, Kim ER, Kim DJ, Lee H. Synthesis of metal-azo dyes and their optical and thermal properties as recording materials for DVD-R. Bulletin of the Chemical Society of Japan 2002;75(9):2067–70.
[14] Song HF, Chen KC, Wu DQ, Tian H. Synthesis and absorption properties of some new azo-metal chelates and their ligands. Dyes and Pigments 2004;60:111–9.
[15] Gan FX, Hou LS. High density optical discs for audio, video and image applications. Proceeding of SPIE 2003;5060:1–6.
[16] Chang D, Yoon D, Ro M, Hwang I, Park I, Shin D. Synthesis and characteristics of protective coating on thin cover layer for high density-digital versatile disc. Japanese Journal of Applied Physics 2003;42(2B):754–8.
[17] Huang TT, Lu YJ, Liao WY, Huang CL. Blue violet laser write-once optical disk with coumarin derivative recording layer. IEEE Transactions on Magnetics 2007;43(2):867–9.
[18] Takashi M, Yutaka K. Optical recording medium, metal complex compound and organic dye compound. WO 2006104196, 2006.
[19] Horie M, Kurose Y, Kubo H, Kiyono K. Optical recording medium and optical recording method of the same. WO2006009107, 2006.
[20] Takashi M, Hisashi S, Kenichi S, Mayumi K, Naoyuki U, Hideki T. Optical recording medium, optical recording material and metal complex compound. WO2007007748, 2007.
[21] Chen LY, Feng XW, Su Y, Ma HZ, Qian YH. Design of a scanning ellipsometer by synchronous rotation of the polarizer and analyzer. Applied Optics 1994; 33:1299–305.
[22] Chen LY, Feng XW, Su Y, Ma HZ, Qian YH. Improved rotating analyser-polarizer type of scanning ellipsometer. Thin Solid Films 1993;234:385–9.
[23] Ertan N. Synthesis of some hetarylazopyrazolone dyes and solvent effects on their absorption spectra. Dyes and Pigments 1999;44:41–8.
[24] Szymczyk M, El-Shafei A, Freeman HS. Design, synthesis, and characterization of new iron-complexed azo dyes. Dyes and Pigments 2007;72:8–15.
[25] Bâtiu C, Panea I, Ghizdavu L, David L, Pellascio SG. Divalent transition metal complexes 4-(4-ethoxy-phenylhydrazone)-1-phenyl-3-methyl-1H-pyrazolin-5(4H)- one. Journal of Thermal Analysis and Calorimetry 2005;79:129–34.
[26] Karcõ F, Karcõ F. The synthesis and solvatochromic properties of some novel heterocyclic disazo dyes derived from barbituric acid. Dyes and Pigments 2008;77:451–6.
[27] Kirkan B, Gup R. Synthesis of new azo dyes and copper(II) complexes derived from barbituric acid and 4-aminobenzoylhydrazone. Turkish Journal of Chemistry 2008;32:9–17.
[28] Christie RM, Dryburgh WT, Standring PN. Some monoazoacetoacetanilide pigments derived from heterocyclic diazo components. Dyes and Pigments 1991;16:231–40.
[29] Karcı F, Ertan N. Hetarylazo disperse dyes derived from 3-methyl-1-(30,50-dipiperidino-s-triazinyl)-5-pyrazolone as coupling component. Dyes and Pigments 2002;55:99–108.
[30] Peng Q, Li M, Gao K, Cheng L. Hydrazone-azo tautomerism of pyridine azo dyes: part 1 – NMR spectra of tautomers. Dyes and Pigments 1990;14(2):89–99.
[31] Peng Q, Li M, Gao K, Cheng L. Hydrazone-azo tautomerism of pyridone azo dyes: part III – effect of dye structure and solvents on the dissociation of pyridone azo dyes. Dyes and Pigments 1992;18:271–86.
[32] Huang FX, Wu YQ, Gu DH, Gan FX. Spectroscopic and thermal properties of short wavelength metal(II) complexes containing α-isoxazolylazo-β-diketones as co-lignads. Spectrochimica Acta Part A 2005;61:2856–60.
[33] Song HF, Chen KC, Tian H. Synthesis of novel dyes derived from 1-ethyl-3-cyano-6-hydroxy-4-methyl-5-amino-2-pyridone. Dyes and Pigments 2002; 53:257–62.
[34] Agarwal RK, Prasad S. Synthesis, spectroscopic and physicochemical characterization and biological activity of Co(II) and Ni(II) coordination compounds with 4-aminoantipyrine thiosemicarbazone. Bioinorganic Chemistry Applications 2005;3:271–88.
[35] Ropret P, Centeno SA, Bukovec P. Raman identification of yellow synthetic organic pigments in modern and contemporary paintings: reference spectra and case studies. Spectrochimica Acta Part A 2008;69:486–97.
[36] Gaber M, El-Baradie KY, El-Sayed YSY. Spectral and thermal studies of 4-(1H-pyrazolo {3,4-d} pyrimidin-4-ylazo) benzene-1,3-diol complexes of cobalt(II), nickel(II) and copper(II). Spectrochimica Acta Part A 2008;69:534–41.
[37] Abdel-Latif SA, Hassib HB. Studies of Mn(II), Co(II), Ni(II) and Cu(II) chelates with 3-phenyl-4-(p-methoxy-phenylazo)-5-pyrazolone. Journal of Thermal Analysis and Calorimetry 2002;68:983–95.
[38] Omar MM, Mohamed GG. Potentiometric, spectroscopic and thermal studies on the metal chelates of 1-(2-thiazolylazo)-2-naphthalenol. Spectrochimica Acta Part A 2005;61:929–36.
[39] Issa RM, Khedr AM, Rizk HF. UV-vis, IR and ^{1}H NMR spectroscopic studies of some Schiff bases derivatives of 4-aminoantipprine. Spectrochimica Acta Part A 2005;62:621–9.
[40] Gup R, Giziroglu R, Kõrkan B. Synthesis and spectroscopic properties of new azo-dyes and azo-metal complexes derived from barbituric acid and amino-quinoline. Dyes and Pigments 2007;73:40–6.
[41] Griffiths J. Colour and constitution of organic molecules. Translated by Hou YF, Wu ZW, Hu JZ. Beijing: Chemistry Industry Press; 1985. p. 202.
[42] Wu YQ, Gu DH, Gan FX, Wang JD, Chen NS. Optical constants of palladium phthalocyanine derivative thin films. Chinese Physics Letters 2002;19:1700–2.
[43] Holtslag AHM, McCord EF, Werumeus Buning GH. Recording mechanism of overcoated metallized dye layers on polycarbonate substrates. Japanese Journal of Applied Physics 1992;31:484–93.
[44] Huang FX, Wu YQ, Gu DH, Gan FX. Optical parameters and absorption of copper (II)-azo complexes thin films as optical recording media. Thin Solid Films 2005;483:251–6.
[45] Campoy-Quiles Heliotis M, Xia GR, Ariu M, Pintani M, Etchegoin P, Bradley DDC. Ellipsometric characterization of the optical constants of polyfluorene gain media. Advanced Functional Materials 2005;15:925–33.